Organo-modified LDH fillers endowing multi-functionality to bio-based poly(butylene succinate): An extended study from the laboratory to possible market

Adam Marek, Vincent Verney, Grazia Totaro, Laura Sisti, Annamaria Celli, Nicole Bozzi Cionci, Diana Di Gioia, Laurent Massacrier, Fabrice Leroux

Organo-modified LDH fillers endowing multi-functionality to bio-based poly(butylene succinate) : an extended study from the laboratory to possible market

Adam A. Marek,[*,a,b] Vincent Verney,[a] Grazia Totaro,[c] Laura Sisti,[c] Annamaria Celli,[c] Nicole Bozzi Cionci,[d] Diana Di Gioia,[d] Laurent Massacrier,[e] Fabrice Leroux [*,a]

[a] *Université Clermont Auvergne, CNRS, Institut de Chimie de Clermont-Ferrand (ICCF), F-63000 Clermont-Ferrand, France*
[b] *Silesian University of Technology, Department of Chemical Organic Technology and Petrochemistry, 44-100 Gliwice, Poland*
[c] *Università di Bologna, Dipartimento di Ingegneria Civile, Chimica, Ambientale e dei Materiali, 40131 Bologna, Italy*
[d] *Università di Bologna, Dipartimento di Scienze e Tecnologie Agroambientali, 40127 Bologna, Italy*
[e] *GBCC, Green Business and Consulting Company, 63800 Cournon d'Auvergne, France*

Graphical Abstract

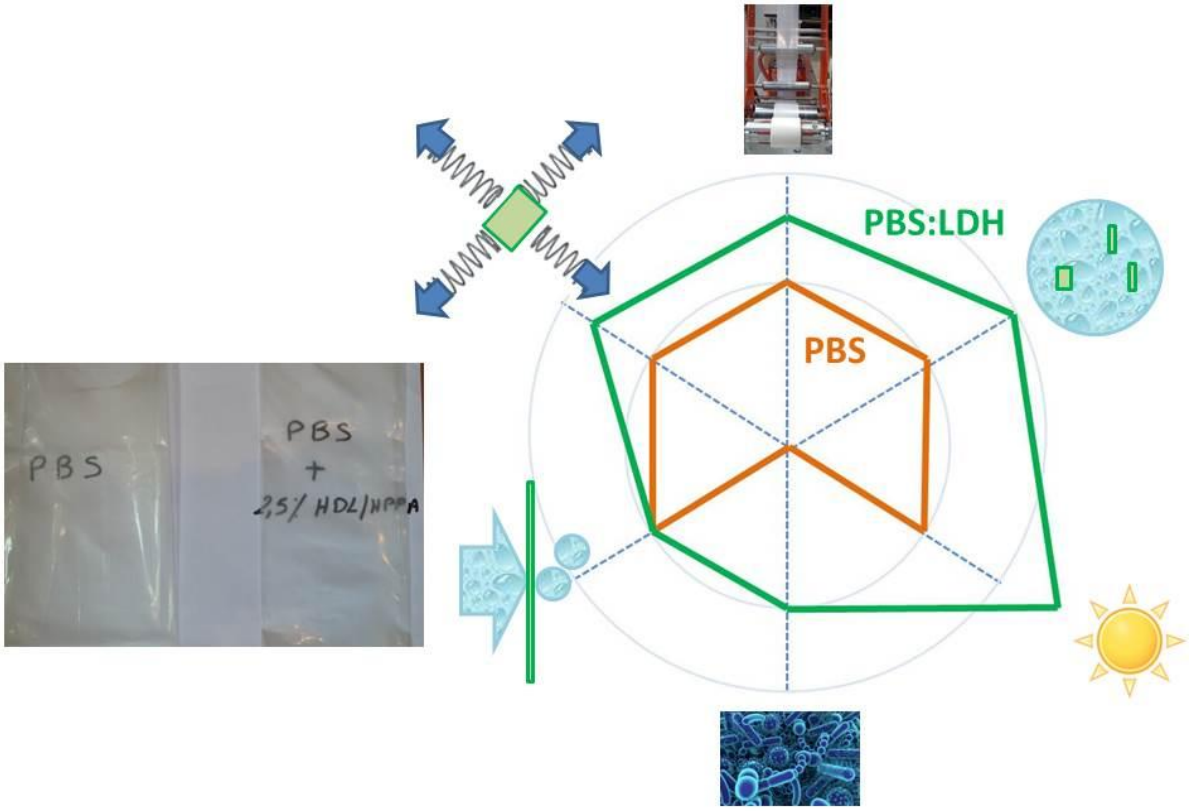

Highlights

- Organo-modified LDH as filler for bio-based polyester
- LDH hybrid filler endowing polymer with multi-functionality
- Chain extension and stability against UV, hydrolysis and bacteria
- Enhanced processability and durability of the polymer composite
- Scale-up and applicability addressed

Keywords: layered double hydroxide; organo-modified filler; polymer nanocomposites; rheology; antibacterial properties

ABSTRACT

Polybutylene succinate (PBS) were processed in melt extrusion by dispersion of organo-modified layered double hydroxide (LDH). Depending on the organic anion interleaved into LDH fillers (L-tyrosine (TYR), L-tryptophan (TRP), L-ascorbate (ASA) and 3-(4-hydroxyphenyl)propionate (HPP)), it was possible to control and tune the properties of the resulting PBS composites. Each LDH filler is found to act differently toward PBS, thus modifying its viscoelastic properties (as expressed by a chain extending effect), its rate of hydrolysis and photo-degradation or its antibacterial activity. The highest chain extending effect was observed in the case of LDH with L-tryptophan, the worst – with L-ascorbate anion. However, L-ascorbate anions interleaved into LDH present 100% activity in antibacterial properties. A better compromise may be achieved when PBS is mixed with different LDHs such as those combining HPP and ASA, making possible to target efficiently multi-properties such as small rate of hydrolysis, photo-stability, biocide activity as well as chain extension, thus turning to a multifunctional (bio)nanocomposites with new possible applications. Finally, a possible scale-up is demonstrated on thin films.

1. INTRODUCTION

Polymers are one of the most important used materials in the world globalizing a whole production estimated at 311 million tons in 2014 and expected to double again in 20 years.

About 26% of this total volume is used in packaging domains, for mostly single-use products (The New Plastics Economy, 2016). Because still, a large majority is classical petroleum-based polymers associated to their long-time natural degradation process, topical problems must be faced concerning their collection, recycling or re-disposal (PSW - plastic solid waste) (Al-Salem et al., 2010).

An alternative solution more sustainable may be the replacement of petroleum-based polymers by eco-friendlier and renewable materials like bio-based aliphatic polyesters which are more and more often used in products (Demirkaya et al., 2015; Rhim et al., 2013). One of the most promising member is poly(butylene succinate) (PBS), semi-crystalline polymer obtained by the direct poly-condensation of succinic acid (bio-based) and butane-1,4-diol (partially bio-based). Due to its thermal properties like glass transition temperature (–34 °C) and relatively high melting point (around 115 °C) close to some poly(olefins) such as poly(propylene), PBS can be processed through usual extrusion, injection molding and thermo-forming processes, this is of great interest since it guarantees direct industrial transfer. Moreover, via copolymerization with other diols and dicarboxylic acids, or by the addition of organic and inorganic fillers, the properties of PBS can be significantly improved, thus making PBS possible to replace classical polymers in a wide range of applications (Kim et al., 2005; Gigli et al., 2016).

In the last decades, a special attention has been paid to layered double hydroxides (LDHs), also known as anionic clays or hydrotalcite-like materials. These materials can be described with the general formula $[M^{II}_{1-x}M^{III}_{x}(OH)_2](A^{n-}_{x/n})\cdot mH_2O$, where M^{II} is a divalent cation (like Mg, Zn, Ni, Cu or Co) and M^{III} is a trivalent cation (like Al, Cr or Fe), and A^{n-} represents inorganic anion such as NO_3^-, CO_3^{2-} or an organic anion. These metal cations $M(OH)_6$ form the positively charged layer by edge-sharing their octahedral, and with diverse charge-compensating anions

78 present in the interlayer space (Rives et al., 1999). By combining both cation and anion
79 versatilities, the resulting compositions are limitless in designing new hybrid LDH assemblies.
80 Often designed as toolbox, such organo-modified LDH may be adapted as nanofillers for
81 different types of polymer including bio-polymer to yield new polymer nanocomposites and thus
82 endowing them with enhanced target properties (Xie et al., 2016; Totaro et al., 2017; Coelho et
83 al., 2012).

84 In the present paper, a family of multifunctional PBS nanocomposites adopting organo-
85 modified Mg-Al LDHs as filler are characterized, that may be potentially used in packaging
86 domains. In the same vein, Costantino et al. have demonstrated the active antimicrobial activity
87 of benzoate organic derivatives intercalated into Zn_2Al and dispersed into poly(ε-caprolactone)
88 (Costantino et al., 2009). Here, the LDHs nanofillers were obtained by the straightforward co-
89 precipitation method with anions coming from 3-(4-hydroxyphenyl)propionate (HPP), L-
90 ascorbate (ASA) and amino acids: L-tyrosine (TYR) and L-tryptophan (TRP). Such selection is
91 explained by the fact that HPP interleaved molecules provide an effective chain extender toward
92 PBS when hosted by Mg-Al LDH structure (Totaro et al., 2017) as well as developing some
93 antioxidant and antibacterial activities (Sun et al., 2016). The other candidates, ASA molecule
94 (called vitamin C) is known as an antioxidant and free radical scavenger. Its key role in the
95 body's life includes to protect the immune system (destroy tumour cells), the cardiovascular
96 system (support the fat metabolism) (Aisawa et al., 2007), while the amino acids TYR and TRP
97 may supply anti-UV properties and polymer chain extension (Coelho et al., 2012).

98 Having in mind such combination of properties potentially available, the synthesized LDHs
99 assemblies were dispersed into PBS by melt extrusion process. The resulting PBS composites
100 were scrutinized to determine the chain extension effect, photo- and hydro-stability as well as the

antibacterial activity against *Escherichia coli* and *Staphylococcus aureus*. Some trends are featured in terms of correlation between the rheological properties (Newtonian viscosity η'_0 associated to the chain extension effect) and the antibacterial properties, as well as between η'_0 before and after photo-aging and the hydrolysis processes. This comprehensive analyses should help to underline the multifunctional properties of the obtained PBS nanocomposites with potential use for food packaging applications and others. Indeed, a scale-up of 30,000 g of a composite Mg_2Al/HPP : PBS (2 wt. % dry filler) is easily achieved, however in adopting the «slurry» method for a better dispersion of state, thus yielding to thin film that is found to exhibit similar modulus, maximum at strain and water vapor transmission rate (WVTR), but extension as well as tearing greater than PBS free of filler.

2. EXPERIMENTAL SECTION

2.1. Materials. Sodium hydroxide, aluminium nitrate $Al(NO_3)_3 \cdot 9H_2O$, magnesium nitrate $Mg(NO_3)_2 \cdot 6H_2O$, sodium nitrate $NaNO_3$ and the guest molecules: L-tyrosine (TYR), L-tryptophan (TRP), L-ascorbic acid (ASA) and 3-(4-hydroxyphenyl)propionic acid (HPP) were purchased from Sigma-Aldrich Chemical. PBS (PBE003) and PuralMg61 were purchased from NaturePlast and Sasol Germany GmbH, respectively. Plate Count Agar (PCA), Nutrient Broth (NB) were supplied from Oxoid, Basingstoke, UK and phosphate buffer solution was purchased by Merck, Darmstadt, Germany. All the materials were reagent grade and used as received. The molecular structures of organic quest molecules are presented at **Scheme 1**.

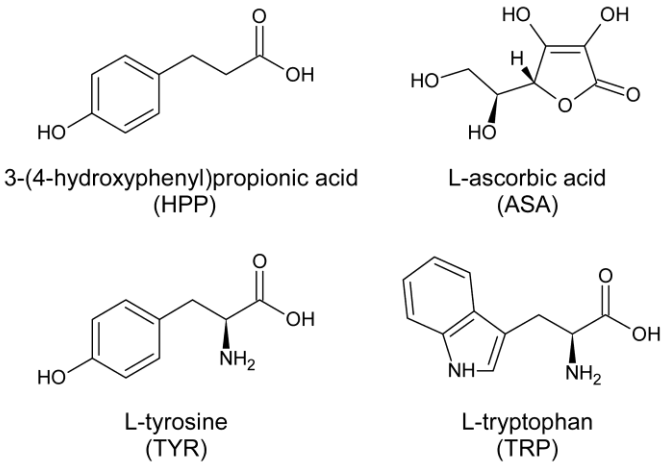

121

122 **Scheme 1**. The organic quest molecular structures.

123 **2.2. Synthesis of layered double hydroxides.** The host substances Mg-Al LDHs with general
124 formula $Mg_2Al(OH)_6[A]\cdot 2H_2O$ (A = HPP, ASA, TYR or TRP) were prepared using so-called
125 co-precipitation method with an initial metal cation feed of Mg:Al of 2 and A:Al of 4.
126 $Al(NO_3)_3\cdot 9H_2O$, and $Mg(NO_3)_2\cdot 6H_2O$ were mixed with milliQ water (100 mL) and added
127 dropwise to the 50 mL solution of organic guest in water. The reaction was carried out with
128 vigorous stirring and under nitrogen atmosphere to avoid contamination by carbonate during 3.5
129 h. The pH was kept constant (9.5–11.0 ± 0.1) with the addition of NaOH solution. After 3.5 h,
130 the salts addition was finished and the reaction mixture was aged for next 3.5 h at room
131 temperature. The final products were centrifuged, washed with deionized water and dried at 40
132 °C in vacuum-oven for 24 h.

133 **2.3. Melt compounding.** PBS/LDH composites were obtained by a melt extrusion process in a
134 twin screw extruder Hakke MINILAB microcompounder (Thermo Electron Corporation). The
135 process was performed at 120 °C, with a roller speed of 100 rpm over 5 min.

136 **2.4. Grinding-homogenization process.** Homogenized LDH fillers and PBS/LDH composites
137 were grinded in Retsch CryoMill machine. Prior to dispersion, LDH fillers were sieved to obtain
138 fraction with particles size below 50 μm.

2.5. Film making. PBS/LDH composite films with thickness about 90–100 μm, used in hydrolysis and photodegradation studies, were prepared by compression moulding. About 0.5 g of composites were placed between two Teflon sheets for one minute under 100 bars at 120 °C.

2.6. Hydrolysis procedure. PBS and PBS/LDH composite films were placed into glass pots with deionized water, purged with nitrogen and closed in the dark in an oven at 35 and 50 °C. These processes were performed two times, separately for succinic acid analysis (by ionic chromatography) and for rheological measurements.

2.7. Photodegradation procedure. PBS and PBS/LDH composite films were placed on a rotating carousel in a SEPAP 12/24 chamber from ATLAS. This apparatus is equipped with four 400 W mercury lamps with $\lambda > 300$ nm light and allows for study the accelerated photo-degradation of polymer. The conditions used in experiments were air atmosphere and 60 °C.

2.8. Antibacterial analysis. The antimicrobial activity of LDHs and PBS composites was assessed by evaluating the survival of bacterial cells (*Escherichia coli* ATCC 11105 and *Staphilococcus aureus* ATCC 6538) in contact with samples. The bacterial culture obtained in NB Medium and aerobic atmosphere for 16 h at 37 °C was next centrifuged at 7000 rpm for 10 min, washed in sterile phosphate buffer solution and re-suspended in the same buffer in order to obtain about 105 colony forming unit per milliliter (CFU mL^{-1}).

The experiments on both LDHs and PBS composites were performed using 50 mg of sieved samples placed into an Eppendorf with 500 μl of cells (105 CFU mL^{-1} in phosphate buffer) at 23 ± 1 °C, gently shaken at 30 rpm for 24 h. After the incubation period, each sample was diluted (1:10) and the dilutions were plated on PCA medium. After incubation of the plates at 37 °C for 24 h, the number of colonies corresponding to the number of viable cells was determined, after averaging using triplicates, through a modification of the equation as follow (Lala et al., 2007):

Inhibition % = ((B–A))/B × 100 (1)

Where inhibition % = percentage of reduction of viable cells, A = average number of viable cells obtained after 24 h of contact with compound powders, and B = average number of viable cells after 24 h of incubation with reference substance. The reference substance was a commercial LDH sample (PuralMg61) and commercial PBS (PBE003).

2.9. Characterization methods. Infrared spectra were recorded using Thermo Scientific Nicolet 6700 FT-IR spectrometer, in the range from 400 to 4000 cm^{-1} and with a resolution of 4 cm^{-1}. Spectra for LDH substances were obtained using thin KBr pellets and the PBS and polymer composites were analyzed as films.

X-ray powder diffraction (XRD) patterns of LDH filers and PBS composites were recorded using a Philips X-Pert Pro diffractometer with Cu-Kα radiation. Data were collected in the range from 2.0° to 70.0° (2θ), with a step size of 0.03° (2θ) and a counting time of 10 s per step.

UV-vis spectra were recorded using Shimadzu UV-2101 PC spectrophotometer. In the case of LDH fillers, the diffuse reflectance spectra were transformed to absorption spectra using Kubelka–Munk theory.

Fluorescence spectra of polymer composites were recorded with a Perkin-Elmer LS-55 luminescence spectrophotometer equipped with a front surface accessory and a pulsed xenon excitation source at 280 nm. Emission data were collected with the monochromator from 200 to 600 nm at a speed scan of 600 nm min^{-1}.

Thermal properties of LDH fillers and PBS composites were characterized by differential scanning calorimetry (DSC), using Perkin-Elmer DSC6 apparatus. The analyses were carried out under nitrogen and firstly, the samples (ca. 10 mg) were heated from 40 to 150 °C at 20 °C/min, kept at high temperature for 2 min and then cooled down to –60 °C at 10 °C/min. After that, the

thermal history of samples was deleted and 2nd scan was performed, by heating from –60 °C to 150 °C at 10 °C/min. The glass transition temperature (T_g), the melting temperature (T_m) and the enthalpy of fusion (ΔH_m) were measured from 2nd scan. T_g was taken as the midpoint of the heat capacity increment associated with the glass-to-rubber transition. The crystallization temperature (T_c) and the enthalpy of crystallization (ΔH_c) were measured during the cooling scan.

Thermogravimetric analysis (TGA) of LDH fillers and composites, was performed in air atmosphere (gas flow 30 mL/min) using a Perkin Elmer TGA7 apparatus. The temperature range from 50 to 800 °C and heating rate 10 °C/min were applied. The onset degradation temperatures (T_{onset}) were taken from the intersections of the tangents of the initial points and the inflection points. The 10% mass loss temperatures (T^{10}_D) were also measured.

The melt rheological properties of the polymer composites were measured in oscillatory frequency sweep mode at 120 °C, using a dynamic mechanical spectrometer (ARES Rheometric Scientific T&A Instruments) equipped with two parallel plate-holders. Diameter of both plates was 8 mm and the gap during measurement was 1 mm. In all cases, the range of frequency sweeps was from 0.1 to 100 rad/s and the oscillatory shear stress amplitude was checked to perform measurement inside the linear viscoelastic domain. The storage modulus (G'), loss modulus (G") and tan δ (ratio of G' and G") were monitored automatically against frequency.

The concentration of succinic acid was measured by ionic chromatography method, using a Thermo Scientific ICS5000 apparatus with conductivity detector, self-regenerating suppressor (SRS) and columns: AS18 2x250 and AG18 2x50 (guard-column). Samples (250 μL) were analyzed at 40 °C, with a flow rate of 0.25 mL/min and run time 35 min. The initial eluent concentration during analysis was changed according to T_0: 10, T_4: 11, T_{11}: 17, T_{21}: 19.5 and $T_{23.1}$: 10 mM KOH /L.

2.10. Scale-up and characterization of the obtained thin films. LDH/HPP material was scaled-up to yield about 600 g of powder mass. To avoid any particle aggregation during the polymer processing, the filler LDH/HPP was mixed with glycerol and water in a mass ration LDH/HPP : glycerol : water of 1:1:3. The mixing was performed in an Ultra Turax during 45' at 8,000 rpm. Extrusion was performed by a twin-screw Clextral BC21 and the slurry was incorporated by pumping (DKM, feeding zone Z2/Z3), and feeding speed of 10,000 g/h for PBS granulates and 750 g/h for LDH slurry, this to reach a filler loading of 2.5 wt. %. The extruded polymer and filler was dried during 2 h at 70°C. The resulting film thickness, performed with a monoloyer extrusion line (EuRexMa XTR20) was of 35 μm and 25 μm for PBS free of filler. Barrier effect at the water vapor (WVTR) was measured using the norm EN NF ISO 2528 at 38 °C and 90% humidity rate (HR).

3. RESULTS AND DISCUSION

3.1. LDH fillers characterization. The organo-modified Mg_2Al/A LDH assemblies (A = HPP, ASA, TYR or TRP) subsequently used in PBS nanocomposites, were prepared by co-precipitation method with intercalation of organic molecules: 3-(4-hydroxyphenyl)propionate (HPP), L-ascorbate (ASA) anions and amino acids: L-tyrosine (TYR) and L-tryptophan (TRP). They present structural features characteristic of layered system as shown by their XRD patterns (**Fig. 1**) together with LDH/nitrate used as reference.

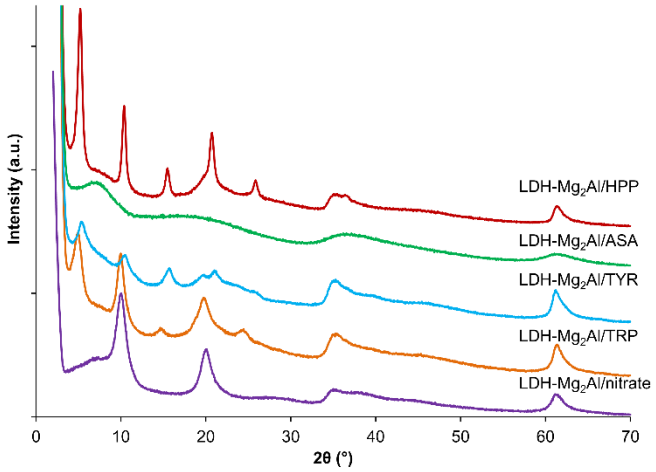

228

229 **Fig. 1.** XRD patterns of Mg_2Al/A (A = HPP, TRP, TYR, ASA, nitrate) organo-modified LDHs.

230 Indeed, LDH/A structural host guest assemblies present XRD patterns with narrow and
231 symmetric (00ℓ) harmonic peaks at low angle. They correspond to the basal spacing (d-value) and
232 indicate higher order reflections, resulting from a high degree of platelets stacking. This is not
233 the case for Mg_2Al/ASA that exhibits wide reflection peaks. Some authors suggest, that the
234 molecules ASA may be arranged horizontally between LDH sheets and with the hydroxyl groups
235 (OH^-) co-intercalated as well. The latter fact may contribute to the ill-organized stacking
236 arrangement (Aisawa et al., 2007).
237 It can be noticed, that Mg_2Al/nitrate LDH shows basal reflections at low 2θ angles leading a
238 d001-value of 0.84 nm. The uptake of organic guest into LDH structure causes an increase of the
239 interlayer space. The chemical composition as well as the cell parameters are summarized (**Table**
240 **1**).

241

242 **Table 1.** Chemical compositions and cell parameters of the organo-modified LDHs

Sample	Chemical composition[a)]	Interlayer	c=3c'	d_{110}	a=2d_{110}

		distance $c'=d_{003}$ (nm)[b)]	(nm)[c)]	(nm)[d)]	(nm)[e)]
PuralMg61	$[Mg_{0.61}Al_{0.39}(OH)_2](CO_3^{2-})_{0.195}$ $0.46H_2O$	0.77	2.31	0.152	0.304
Mg_2Al/nitrate	$[Mg_{0.66}Al_{0.33}(OH)_2](NO_3^-)_{0.37}$ $0.74H_2O$	0.84	2.52	0.151	0.302
Mg_2Al/HPP	$[Mg_{0.66}Al_{0.33}(OH)_2](HPP^-)_{0.23}$ $0.19H_2O$	1.68	5.04	0.151	0.302
Mg_2Al/ASA	$[Mg_{0.66}Al_{0.33}(OH)_2](ASA^-)_{0.36}$ $0.22H_2O$	1.24	3.72	0.151	0.302
Mg_2Al/TYR	$[Mg_{0.66}Al_{0.33}(OH)_2](TYR^-)_{0.31}$ $0.19H_2O$	1.66	4.98	0.151	0.302
Mg_2Al/TRP	$[Mg_{0.66}Al_{0.33}(OH)_2](TRP^-)_{0.32}$ $0.15H_2O$	1.80	5.40	0.151	0.302

a) Anion and water content were determined by TGA (i.e. molar mass).

b) Determined by the 003 reflection in XRD analysis.

c) Total thickness of the brucite-like layers and the interlayer distance.

d) Determined by the 110 reflection in XRD analysis.

e) Lattice parameter related to the cation-cation distance.

The cell parameter **a**, calculated from the position of the reflection (*110*), indicates any deviation from the stoichiometry with respect to the structural references (here Mg-Al/nitrate) (Cavani et al., 1991). For the obtained O/I LDHs, a value of **a** is 0.302 nm. In comparison to the nitrate reference, this value confirms a constant cation ratio Mg:Al of 2. It is worth to mention the absence of contamination by LDH/carbonate phase.

FTIR spectra of Mg_2Al LDH hybrids are presented in **Fig. S1**. The observed bands confirm the presence of anions and the position of the vibration bands agrees with literature (Totaro et al., 2017; Gao et al., 2013; Wei et al., 2005).

The UV-absorbing properties of Mg-Al LDHs are presented in **Fig. 2**. The nitrate-inorganic derivative, which is used as reference, presents practically no absorption in the UV range. When the organic molecules are inserted into LDH structure, the absorption increases significantly,

especially in the case of ASA and amino acid TRP and TYR, with the maximum absorption of 266, 296 and 303 nm, respectively. In the case of Mg_2Al/HPP, a narrower absorption range with maximum 281 nm is observed. The presented spectra indicate, that these organo-modified Mg-Al LDHs should be effective as potential UV-absorbers. Their UV-stabilizing effect on PBS will be addressed in a next section.

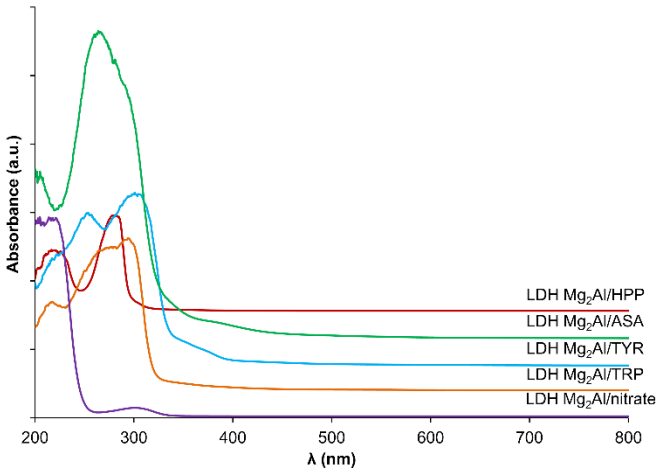

Fig. 2. Diffuse reflectance UV-vis spectra (Kubelka–Munk functions) of organo-modified Mg-Al LDHs.

3.2. PBS-LDH composites characterization. PBS nanocomposites were prepared by melt extrusion with the addition of synthesized Mg-Al LDHs in amount between 2.5 to10 wt. %. The fillers were used individually or as mixture in combination with Mg_2Al/HPP (1:1) which is known as a chain extender in PBS composites (Leroux et al., 2017; Totaro et al., 2017). PBS nanocomposites with 5 wt. % of organo-modified Mg_2Al LDHs and its nitrate reference are characterized by XRD and the associated patterns displayed in **Fig. 3** (summarized in **Fig. S3** for loading of 10 wt. %).

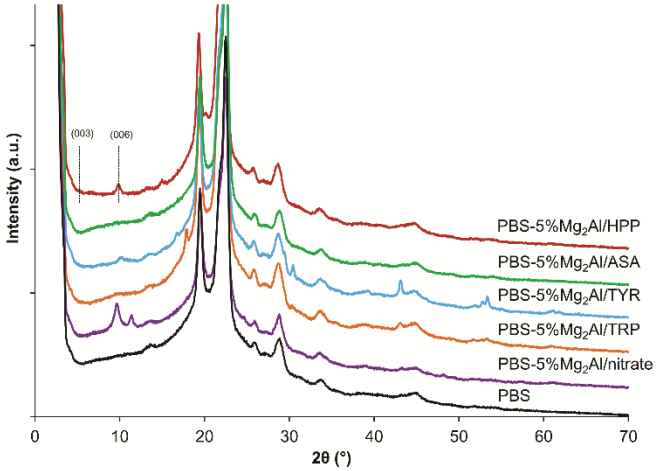

Fig. 3. XRD patterns of PBS and PBS nanocomposites with 5 wt. % of Mg-Al organo-modified LDH fillers.

At first, some reflections are due to the semi-crystalline structure of PBS. Indeed in the 2θ range between 18 and 35°, the following reflections are visible and assigned to (020) (021) (110) (111) of PBS crystal in monoclinic symmetry (Yoo and Im,, 1999). From those reflections, neither their location nor their relative intensity is modified after the incorporation of LDH-based filler. This indicates that the filler loading does not affect the PBS molecular crystal. Secondly, the harmonic peaks arising from the layered structure of LDH are not observed anymore, except for LDH/HPP, for which the (003) and (006) are depicted at 5 and 10 wt. % (**Fig. 3** and **Fig. S3**). The basal reflection (003) is also observed for LDH/nitrate. For Mg_2Al/HPP, the observation of some layered structure remaining after extrusion is not surprising since the LDH structure is initially extensively stacked as observed by its narrow (00ℓ) basal reflections, *i.e.* its large coherence length along the stacking direction. The absence of harmonic peaks for the other compositions suggests an intimate mixture between its layered structure and the polymer chain.

One cannot discard the possible presence of carbonate contamination within LDH in the case of LDH/nitrate loaded as 5 wt. % and of Mg_2Al/HPP as 10 wt. % (**Fig. S3**). As the LDH fillers are initially free of carbonate contamination (Fig. 1), it means that the contamination is occurring during the thermal pretreatment or the exposure to air before their dispersion into PBS and/or during the extrusion process in temperature.

The calorimetric and thermogravimetric data for PBS nanocomposites with Mg-Al LDHs are summarized in **Table 2**, and TGA thermograms of nanocomposites with 5 wt. % of LDHs are shown in **Fig. 4** as example. TGA and DTGA traces for the PBS nanocomposites (with the other filler loadings 2.5 and 10 wt. % and mixtures of LDHs) are shown in the ESI (**Fig. S2**).

Table 2. TGA and DSC results of melt blended PBS nanocomposites with Mg-Al LDHs filler.

Sample	T_{onset} (°C)[a)]	T^{10}_D (°C)[a)]	Res. mass (%)[a)]	T_C (°C)[b)]	ΔH_C (J/g)[b)]	T_g (°C)[c)]	T_m (°C)[c)]	ΔH_m (J/g)[c)]
PBS pure	385	362	0.7	85	63	-31	115	47
PBS-5%Mg_2Al/nitrate	360	327	3.3	85	58	-31	115	48
PBS-5%Mg_2Al/HPP	369	345	3.3	85	54	-32	114	50
PBS-10%Mg_2Al/HPP	363	338	5.0	85	56	-33	114	50
PBS-2.5%Mg_2Al/ASA	370	350	1.8	84	55	-29	116	46
PBS-5%Mg_2Al/ASA	371	347	3.4	86	62	-30	116	49
PBS-10%Mg_2Al/ASA	368	341	5.1	86	52	-29	115	43
PBS-2.5%Mg_2Al/TYR	379	354	1.5	88	62	-29	115	49
PBS-5%Mg_2Al/TYR	376	351	2.6	87	58	-29	115	41
PBS-10%Mg_2Al/TYR	372	344	4.9	84	55	-31	115	43
PBS-2.5%Mg_2Al/TRP	371	351	1.3	86	56	-26	115	47
PBS-5%Mg_2Al/TRP	367	349	2.8	85	56	-33	114	46

PBS-10%Mg_2Al/TRP	371	357	4.5	83	50	-33	114	33
PBS-10%Mg_2Al/HPP:ASA	360	335	2.9	85	53	-33	115	46
PBS-10%Mg_2Al/HPP:TYR	361	337	4.9	84	57	-31	115	48
PBS-10%Mg_2Al/HPP:TRP	357	337	4.1	84	53	-30	114	43

a) Determined by TGA at 10 °C/min in air.

b) Determined by DSC during the cooling scan from the melt at 10 °C/min.

c) Determined by DSC during the 2nd heating scan at 10 °C/min.

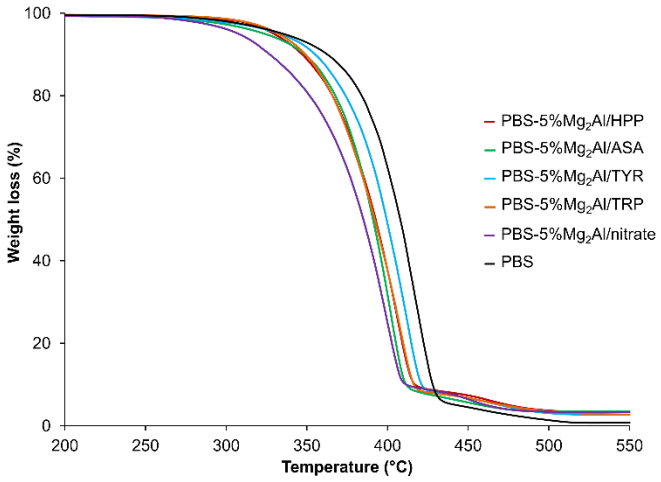

Fig. 4. TGA traces of PBS and PBS nanocomposites with 5 wt. % of Mg-Al organo-modified LDHs.

All nanocomposites exhibit some lower thermal stability than pure PBS, that is characterized by a decrease in T_{onset} (initial temperature of degradation process) and in T^{10}_{D} (temperature at which the material lose 10% of weight). This trend is also observed with increasing the LDH amount. Only in the case of PBS with 10 wt. % of Mg_2Al/TRP LDH, an opposite effect and higher T_{onset} and T^{10}_{D} are observed than for 5 wt. % amount, but still bellow PBS alone. This is probably due to a stronger affinity of the platelets toward the cross-linking reactions with PBS. This was

317 previously noticed for PBS-Mg_2Al/TRP composites but obtained through in-situ polymerization
318 process (Totaro et al., 2018).
319 A complete decomposition occurs in the range 300–450 °C. It is in accordance with the literature
320 (Totaro et al. 2018; Wei et al., 2012) and can be explained by degradation process of PBS, this
321 catalyzed by the metal ions inside the layers as well as the water molecules released during the
322 decomposition.
323

324 **3.3. Chain extending effect.** It is well known that additives may endow polymers with
325 required properties to reach possible application. One of the basic characteristic is the molecular
326 weight and the associated viscoelastic behavior, which can be modified by addition of
327 plasticizers (smaller molecular weight) or chain extenders (higher molecular weight). The latter
328 can also be used during processing polymer condensation as illustrated by PET to avoid negative
329 effect of thermo-hydrolysis reaction during thermomechanical processing (Bimestre et al., 2012).
330 The effect of synthesized LDH fillers on the molecular weight evolution is here examined. It is
331 monitored by rheology in the molten state and described according to the so-called Cole-Cole
332 plot, commonly adopted to scrutinize any variations in the complex viscosity components. By
333 plotting the imaginary viscosity (η") versus real viscosity (η'), a circle arc in the complex plane
334 is observed (Friedrich et al., 1992). Indeed, such representation highlights clearly the polymer
335 composites molecular evolution by fitting the Cole-Cole depressed semi-circle and its
336 extrapolation to the x-axis (η' at η" = 0), the Newtonian zero-shear viscosity $\eta'_{0,}$ which reflects
337 the change in the molecular mass, calculated according to (Mark-Houwink equation, 2007)

338 $$\eta'_0 \propto {M_w}^a \qquad (2)$$

The synthesized Mg-Al LDHs were loaded to PBS matrix in 2.5–10 wt. %. The mixtures of LDHs including Mg_2Al/HPP with another LDH hybrid filler in mass ratio 1:1, are also prepared to possibly tune PBS towards multi-properties. The effect of using nanofillers on PBS chain extension is presented as η" – η' Cole-Cole plots (**Fig. 5**) and the resulting values of the Newtonian zero-shear viscosity are summarized in **Table 3**.

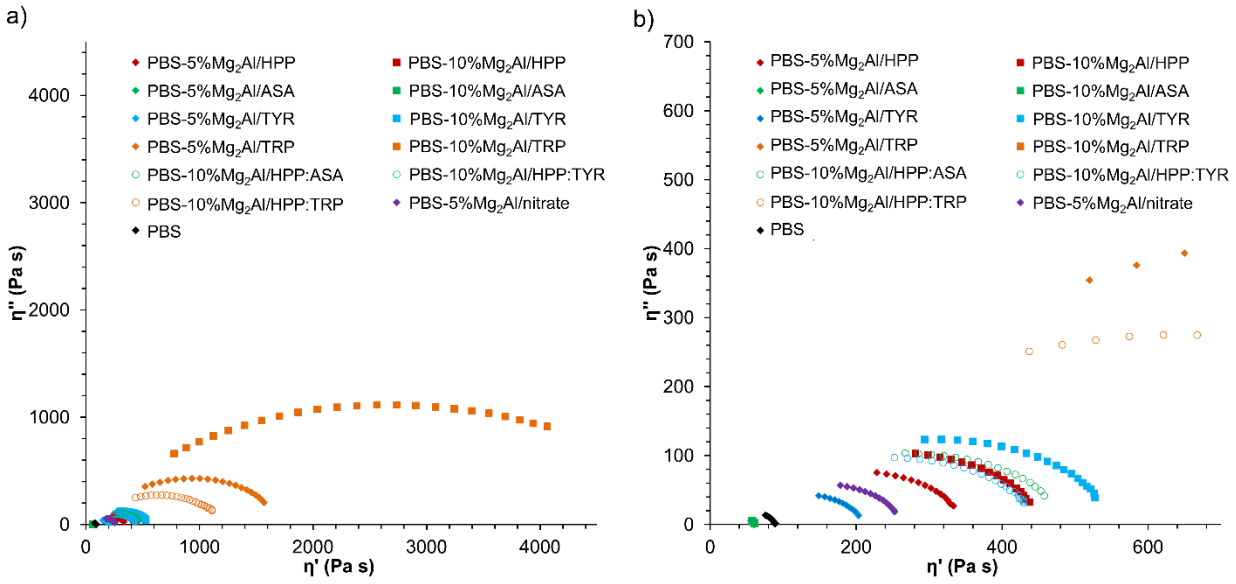

Fig. 5. Cole-Cole plots of (a) PBS and PBS nanocomposites with Mg-Al organo-modified LDH fillers, (b) zoom region in the lower values of viscosity.

Table 3. Newtonian zero-shear viscosity η'_0 for PBS composites as a function of the loadings using Mg-Al organo-modified LDH fillers.

PBS nanocomposites	η'_0 (Pa s) in dependent of LDH amount (wt. %)			
	0	2.5	5	10
PBS pure	90			
PBS-Mg_2Al/nitrate			274	

PBS-Mg_2Al/HPP		365	475
PBS-Mg_2Al/ASA	96	80	82
PBS-Mg_2Al/TYR	91	218	580
PBS-Mg_2Al/TRP	388	1815	5356
PBS-Mg_2Al/HPP:ASA			515
PBS-Mg_2Al/HPP:TYR			470
PBS-Mg_2Al/HPP:TRP			1269

One of the best results is obtained for Mg_2Al/TRP; quantitatively, loaded as low as 2.5 wt. %, the Newtonian zero-shear viscosity is similar to Mg_2Al/HPP, however, using twice the amount. It is worth to mention that the response in η'_0 is not linear as a function of mass loading, since an increase of one order for η'_0 is observed at 10 wt. % between both fillers. The influence of Mg_2Al/TYR is weaker, and in the case of Mg_2Al/ASA, a plasticizing effect is observed. Such differences between LDHs may result from the chemical structures and from the tethered organic molecules as well as the state of dispersion.

3.4. Photo-stability of PBS nanocomposites. PBS and PBS nanocomposites with Mg-Al LDHs were exposed on UV irradiation in accelerated ageing chamber under aerobic conditions at 60 ºC. Since Mg-Al organo-modified LDHs exhibit UV absorption (**Fig. 2**), their derivative PBS composites are expected to be UV-stabilized. The UV-vis transmittance spectra are presented in **Fig. 6**. A better performance as a UV stabilizer is shown in the case of the addition of 10 wt. % of Mg_2Al/TRP into PBS. The transmittance decreases practically to zero in the UV-C range (100–280 nm) and below 40% in the UV-B range (280–315 nm). For the other PBS composites, the efficiency in UV absorption is little less. It is worth to mention that the UV

absorption is not filler loading-dependent and after a certain mass loading (5 wt. %), the effect is constant.

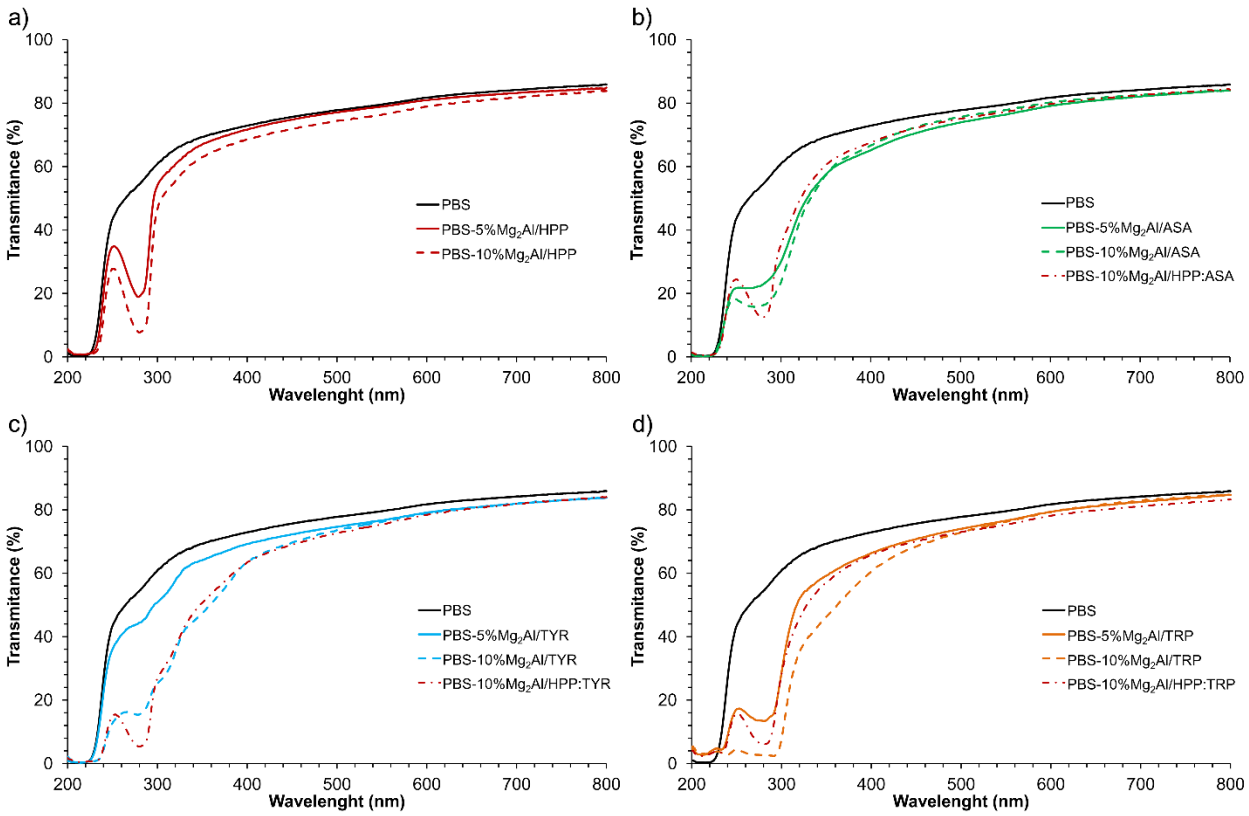

Fig. 6. UV-vis transmittance spectra of PBS and PBS composites with Mg-Al organo-modified LDHs: (a) Mg_2Al/HPP, (b) Mg_2Al/ASA, (c) Mg_2Al/TYR and (d) Mg_2Al/TRP.

The variation of Newtonian viscosity η'_0 during exposure on UV radiation is presented in **Fig. 7**. Pure PBS shows UV-resistance for the first 60 h, then it begins to degrade rather quickly. The addition of Mg_2Al/TYR LDH turns out to be completely ineffective, regardless of the amount used, a slow decrease in viscosity (effect of the photo-degradation) is observed. The other LDH hybrids act as UV-stabilizers during the time period. In the case of composites with 10 wt. % of Mg_2Al/TRP and Mg_2Al/HPP:TRP LDHs mixture, which have the highest Newtonian viscosity, a

further increase in η'_0 is observed, probably due to additional crosslinking reactions. The cross-linking phenomenon in the presence of LDH modified with amino acids like TRP, has recently been depicted (Totaro et al., 2018).

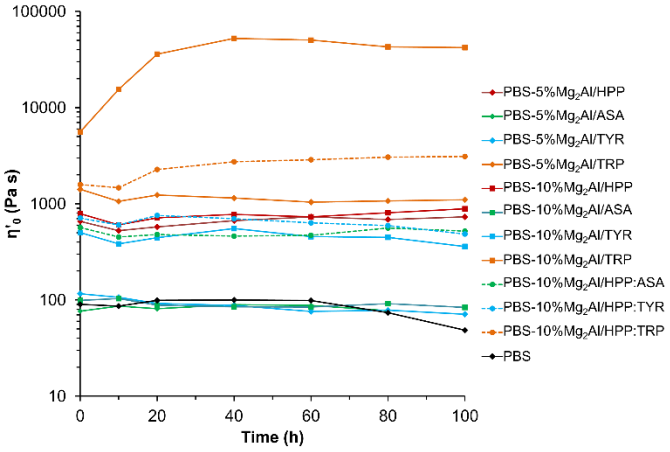

Fig. 7. Evolution of Newtonian zero-shear viscosity η'_0 (in logarithmic scale) versus time for PBS and PBS-Mg-Al LDH composites, during photo-ageing at 60 °C.

UV-vis transmittance spectra of PBS and its nanocomposites with 5 wt. % of Mg-Al LDH, before and during UV radiation, are presented in **Fig. S4**. Pure PBS does not present any UV-sensitive functional groups, and its transmittance spectra are not changed during the process. The dispersion of Mg-Al LDHs into PBS decreases the transmittance band at about 300 nm, however a lower effect is observed for composite with TYR compound. When the samples are irradiated, the transmittance is changed. For the PBS-Mg_2Al/ASA composite, it increases during all time of radiation, while for the other composites a decrease in transmittance is observed during a first period (10–40 h), depending of organic molecule used (TRP, HPP) and then it increases again. This phenomenon may be caused by the transformation of molecules within the LDH structure or by their interaction with the polymer matrix.

399 Significant changes caused by UV on some of the PBS nanocomposites have been also
400 registered using fluorescence spectroscopy (**Fig. S4**), similar to the decrease of UV
401 transmittance, described before.

402 **3.5. Hydrolysis of PBS nanocomposites.** Hydrolysis of PBS and PBS-Mg-Al LDH
403 composites is performed at 35 and 50 °C. The reaction progress is monitored by both; the
404 evolution of Newtonian zero-shear viscosity and the release of succinic acid during hydrolysis.
405 When the process is performed at 35 °C, the Newtonian zero-shear viscosity seems to be quite
406 stable (**Fig. 8**). Only for pure PBS and composites with 5 and 10 wt. % of Mg_2Al/TRP and
407 Mg_2Al/TYR LDHs, the viscosity decreases, however in the case of composites, after 80 h, the
408 value of viscosity is stabilized in contrast to pure PBS.
409

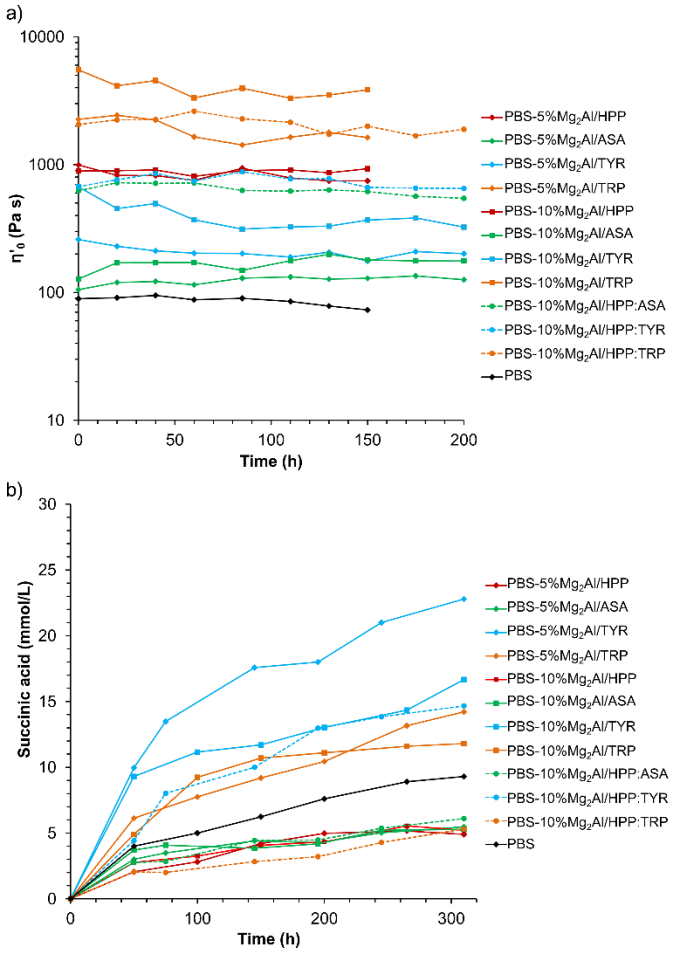

410

411 **Fig. 8.** (a) Evolution of Newtonian zero-shear viscosity (in logarithmic scale) and (b) succinic
412 acid concentration vs time for PBS and PBS-Mg-Al LDH composites, during hydrolysis at
413 35 °C.

414

415 These results can be confirmed by the observation of succinic acid concentration measured by
416 ionic chromatography (**Fig. 8b**). The succinic acid is released most intensively (10–22 mmol/L
417 after 310 h) for all composites with Mg_2Al/TYR LDH and Mg_2Al/TRP LDH used alone. For the
418 other composites, the final concentration is lower of about 1.5 times than for pure polymer and
419 does not exceed 6 mmol/L. The significant viscosity decrease observed for composites with
420 Mg_2Al/TRP and Mg_2Al/TYR during the first hours, is most probably caused by hydrolysis

421 reaction of the polymer. These results are promising for composites with HPP and ASA Mg-Al
422 LDHs. It is also interesting to note that the release in succinic acid is not correlated to the
423 solubility of the anions, of 330, 2.71, 1.4, 11.4 and 58 g/L for ASA, HPP, TYR, TRP and
424 succinic acid, respectively. Counter-intuitively, the greater release of succinic acid is for the less
425 soluble anions such as TYR and TRP, while the smaller release is for the highly soluble ASA
426 anions.
427 The hydrolysis experiment is repeated at 50 ºC and at this temperature, a higher rate of
428 hydrolysis is observed (**Fig. S6 a** and **b**). Once again the composites containing Mg_2Al/TRP and
429 Mg_2Al/TYR LDHs seem to be the less resistant to the aqueous environment. The Newtonian
430 zero-shear viscosity of composites with 5 and 10 wt. % of fillers, after 200 h decreases by 78 and
431 83% for Mg_2Al/TRP and 67 and 52% for Mg_2Al/TYR LDHs, respectively. Even in the case of
432 Mg_2Al/HPP LDH, which is supposed to act as an efficient chain extender, the final η'_0 was 33
433 and 39% of its initial values. However, the temperature 50 ºC is relatively high for packaging
434 materials and the degradation of PBS and LDH fillers is not surprising. The succinate anions
435 content in water (**Fig. S6 b**) is about two times higher than for processes performed at 35 ºC. The
436 highest concentration is detected as previously for Mg_2Al/TYR and 10 wt. % Mg_2Al/TRP PBS
437 composites, with 38 to 48 mmol/L respectively after 310 h of immersion, while the value is
438 about 22 mmol/L for PBS free of filler. The best results (lower content of succinate anions) are
439 obtained for composites with 5 wt. % of Mg_2Al/HPP and those containing Mg_2Al/ASA LDHs.
440
441 **3.6. Antibacterial properties of PBS nanocomposites.** Since packaging includes possibly the
442 contact with food, it is necessary to evaluate the bacteria growth in contact to these materials.
443 The bactericidal activity of synthesized Mg-Al LDHs powders is first examined from tests, using

444 a Gram-positive bacterium, *Staphylococcus aureus* ATCC 6538 (*S. aureus*), and a Gram-
445 negative, *Escherichia coli* ATCC 8739 (*E. coli*), both common food-borne pathogens (Park,
446 2015).

447 Secondly, the antibacterial properties of PBS nanocomposites are scrutinized (**Table 4**). The
448 results are expressed as percentage of viable cells reduced during test, obtained in respect to
449 commercial samples (PBS and PuralMg61) which do not show any antibacterial activity and are
450 used as a reference material.

451

452 **Table 4.** Antibacterial activity of Mg-Al LDH hybrids and PBS nanocomposite powders,
453 expressed as the percentage of reduced viable cells

Sample	*E. coli* ATCC8739 (% inibition)	*S. aureus* ATCC 6538 (% inibition)
PuralMg61	0.0 ± 0.0	0.0 ± 0.0
Mg_2Al/HPP	59.0 ± 3.0	75.0 ± 0.0
Mg_2Al/ASA	100.0 ± 0.0	100.0 ± 0.0
Mg_2Al/TYR	100.0 ± 0.0	100.0 ± 0.0
Mg_2Al/TRP	100.0 ± 0.0	100.0 ± 0.0
PBS pure	0.0 ± 0.0	0.0 ± 0.0
PBS-5%Mg_2Al/HPP	89.0 ± 4.0	94.0 ± 1.3
PBS-10%Mg_2Al/HPP	100.0 ± 0.0	98.0 ± 0.1
PBS-2.5%Mg_2Al/ASA	92.0 ± 1.9	100.0 ± 0.0

PBS-5%Mg_2Al/ASA	95.0 ± 1.5	100.0 ± 0.0
PBS-10%Mg_2Al/ASA	100.0 ± 0.0	100.0 ± 0.0
PBS-2.5%Mg_2Al/TYR	57.0 ± 2.6	14.3 ± 9.0
PBS-5%Mg_2Al/TYR	99.0 ± 0.0	15.0 ± 10.0
PBS-10%Mg_2Al/TYR	100.0 ± 0.0	71.0 ± 10.0
PBS-2.5%Mg_2Al/TRP	56.9 ± 2.7	0.0 ± 0.0
PBS-5%Mg_2Al/TRP	74.4 ± 7.1	23.6 ± 0.0
PBS-10%Mg_2Al/TRP	100.0 ± 0.0	53.5 ± 0.0
PBS-10%Mg_2Al/HPP:ASA	100.0 ± 0.0	99.6 ± 0.0
PBS-10%Mg_2Al/HPP:TYR	96.8 ± 0.4	10.0 ± 1.7
PBS-10%Mg_2Al/HPP:TRP	97.0 ± 0.0	12.0 ± 2.9

All tested Mg-Al LDH hybrid powders show strong antibacterial activity, and in the case of ASA, TYR and TRP, the cell mortality rate is 100% for both: *E. coli* and *S. aureus*. Only Mg_2Al/HPP LDH shows less activity and the inhibition reaches 59 and 75%, respectively. Although all molecules show a similar bactericidal effect, the mechanism of action is different. TRP is known to have a distinct preference for the interfacial region of lipid bilayers and participates in cation–π interactions, due to significant quadrupole moment formed by the extensive π-electron system of the aromatic indole sidechain (Chan et al., 2006). In the case of ascorbic acid (like other antioxidants), the antimicrobial and antiviral activity may be caused by free radicals which are formed during autoxidation mechanism (Salo et al., 1978), while 3-(4-

464 hydroxyphenyl)propionic acid (HPP) has this activity thanks to presence of the *p*-hydroxyl group
465 on the benzyl ring (Sun et al., 2016).

466 When LDHs are dispersed in PBS matrix, an activity is maintained, however, in most of the
467 cases, it is quantity-dependent. The best results are obtained for PBS composites with
468 Mg_2Al/ASA. Its efficiency in inhibiting *E. coli* increases from 92 to 100% for loading 2.5–10 wt.
469 % and the activity against *S. aureus* is 100% for all composites. The more significant impact of
470 the LDH amount is for Mg_2Al/TYR and Mg_2Al/TRP. Indeed, composites with 2.5 wt. % LDH,
471 the antibacterial activity against *E. coli* is similar (about 57% of inhibition), while against *S.*
472 *aureus*, the 14.3% (for Mg_2Al/TYR) and zero activity (0% of inhibition for Mg_2Al/TRP) is
473 observed. The growth of *E. coli* is completely stopped, with 5 wt. % of Mg_2Al/TYR or 10 wt. %
474 of Mg_2Al/TRP. *S. aureus* seems to be more resistant and for the composites with 10 wt. % of
475 amino acid modified LDHs, the inhibition is of 71 and 53.5%, respectively. Interesting results
476 are obtained for composites with Mg_2Al/HPP: in spite of the fact that the hybrid LDH is showing
477 the worse activity in the series against both bacteria, when it is incorporated into PBS, the
478 inhibition increases up to about 100% efficiency with 10 wt. % of LDH loading.

479 Concerning PBS composites with LDH mixtures, around 100% in antibacterial activity against
480 both bacteria is achieved only in the case of PBS-10%Mg_2Al/HPP:ASA. The two other HPP
481 mixtures (with TYR or TRP) are not so efficient. Indeed, in the case of *E. coli*, a synergic effect
482 is however observed as an inhibition higher than for each LDH composition is reached, while the
483 activity against *S. aureus* is much lower and down to about 10% of efficiency. Most probably,
484 some chemical interactions between HPP and amino acids proceed and the mechanism of
485 interaction with bacteria is then disturbed. Indeed, it is possible that the amino groups react with
486 the hydroxyl group of HPP in the confined space, this is illustrated in phenol type molecules

reacting with amino acid and proteins (Bittner, 2006). Further tests are required to confirm this hypothesis.

3.7. The multi-functionality correlation of PBS composites. All previously described results have been correlated together and presented in the triangle form in **Fig. 9**. The top corner presents the value of Newtonian viscosity η'_0 of started materials, the left corner represents η'_0 after 80 h of photo-ageing and in the right corner η'_0 after 80 h of hydrolysis at 50 ºC, respectively. It can be easily noticed, that Mg_2Al/HPP LDH is the best compromise as UV stabilizer to preserve PBS against UV degradation. The effectivity of Mg-Al LDHs with ASA and TYR are worse, and in the case of TRP, a strong crosslinking effect not suitable for polymer processing is observed when it is used in higher amount. On the other hand, Mg_2Al/ASA LDH can be used as an additive with HPP for reducing the rate of hydrolysis as well as the bacteria activity.

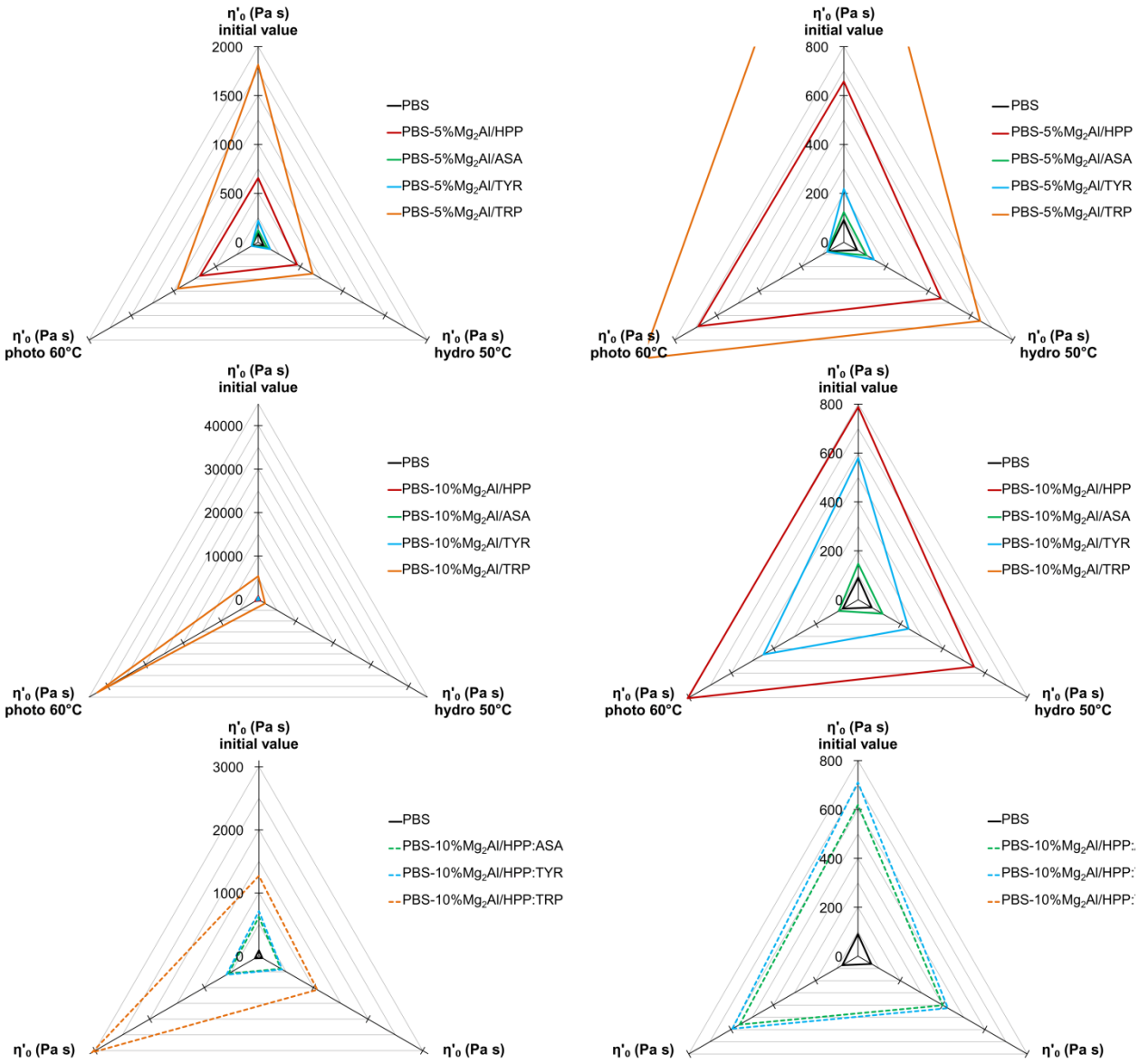

Fig. 9. Radar-type correlation between the Newtonian viscosities η'_0 before and after 80 h in photo-ageing and hydrolysis conditions for PBS and PBS-Mg-Al LDH composites; overall view (right) and zoom region (left).

Fig. 10 displays the correlation of Mg-Al organo-modified LDH between its antibacterial activity and the chain extension effect. All composites with Mg_2Al/ASA and composites with Mg_2Al/HPP or Mg_2Al/TYR LDHs in amount of 5 wt. % (or more) show over 90% inhibition

against *E. coli* bacteria growth (**Fig. 10a**). Mg_2Al/TRP LDH filler may have similar effectiveness if it used in higher amount or in combination with Mg_2Al/HPP. In the case of Gram-positive bacterium like *S. aureus*, the composites with Mg_2Al/ASA and Mg_2Al/HPP LDH are the only compositions efficient, as well as the mixture of the two (**Fig. 10b**).

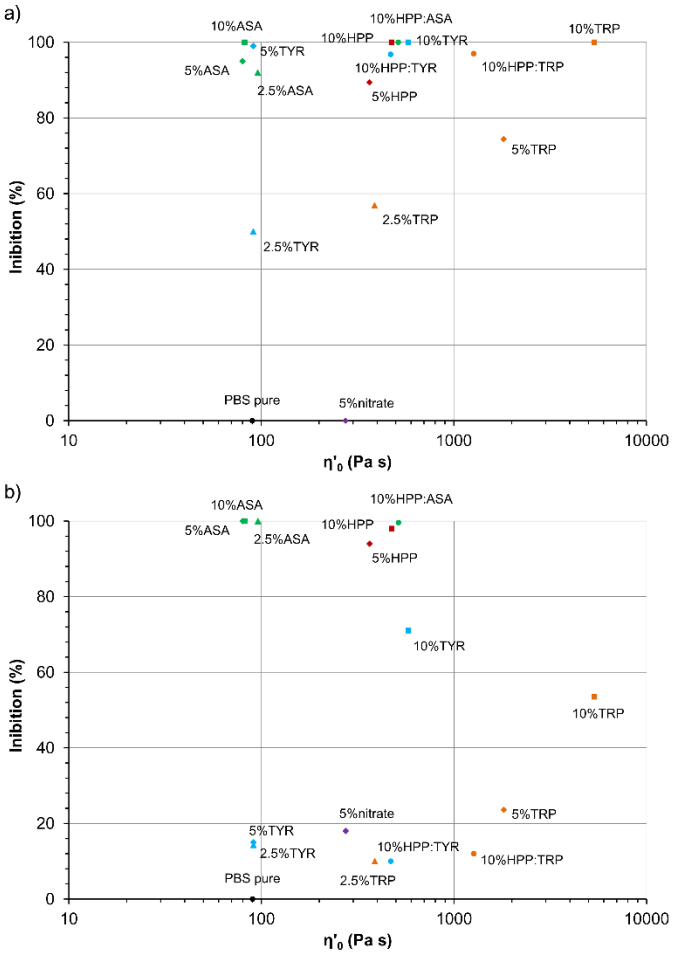

Fig. 10. The correlation of antibacterial effect, expressed as inhibition (%) of bacterial growth against (a) *E. coli* and (b) *S. aureus*, related to the Newtonian viscosity η'_0 (Pa.s).

Although the high antibacterial activity, especially against *E.coli*, can be obtained for these composites, they significantly differ in chain extender effect. The values of Newtonian viscosity

520 is about 100 Pa.s for ASA and TYR (5 wt. %), 600–800 Pa.s for composites with HPP and its
521 mixtures with ASA and TYR, finally over 1000 Pa.s for composites with Mg_2Al/TRP LDH.
522 Thus, the choice of LDH filler should also be determined as a function of the application and its
523 associated required properties.

524 **3.8. Scale-up: toward applicative possibilities**

525 The filler Mg_2Al/HPP is evaluated in PBS in a scale-up process. From the thin films obtained
526 in a larger quantity (process of ≈ 10 kg/h of PBS composites), it is then possible to rationalize the
527 possible applicability. This aspect of our study is unusual, since such consideration is scarcely
528 reported in the literature for polymer composite domain. The thin film PBS-Mg_2Al/HPP presents
529 a good appearance at the extruder outlet (**Fig. 11**) with a haze color as for PBS itself after
530 extrusion process. The composite film exhibits an increase in modulus, maximum at strain,
531 extension as well as enhanced tearing properties compared to PBS itself (**Table 5**). Indeed, an
532 interesting aspect is the tearing properties that is superior (of 25%) in both longitudinal and
533 transversal direction compared to PBS. This is one of the key parameter for its use as thin films
534 for packaging. However, the WVTR remains constant, indicating that even if some mechanical
535 properties are met, the barrier properties remain to be solved.

536 **Table 5**. Mechanical properties and WVTR of thin film of PBS and PBS Mg_2Al/HPP composite

	PBS	PBS composite
Film thickness (μm)	25	35
Modulus (MPa)	410	650
Max at strain (MPa)	35	41
Extension (mm)	2.9	6.1
Tear (N/mm)		

Longitudinal	505	610
Transversal	585	780
WVTR ($g/m^2/day$)	480 ± 4	377 ± 4

537

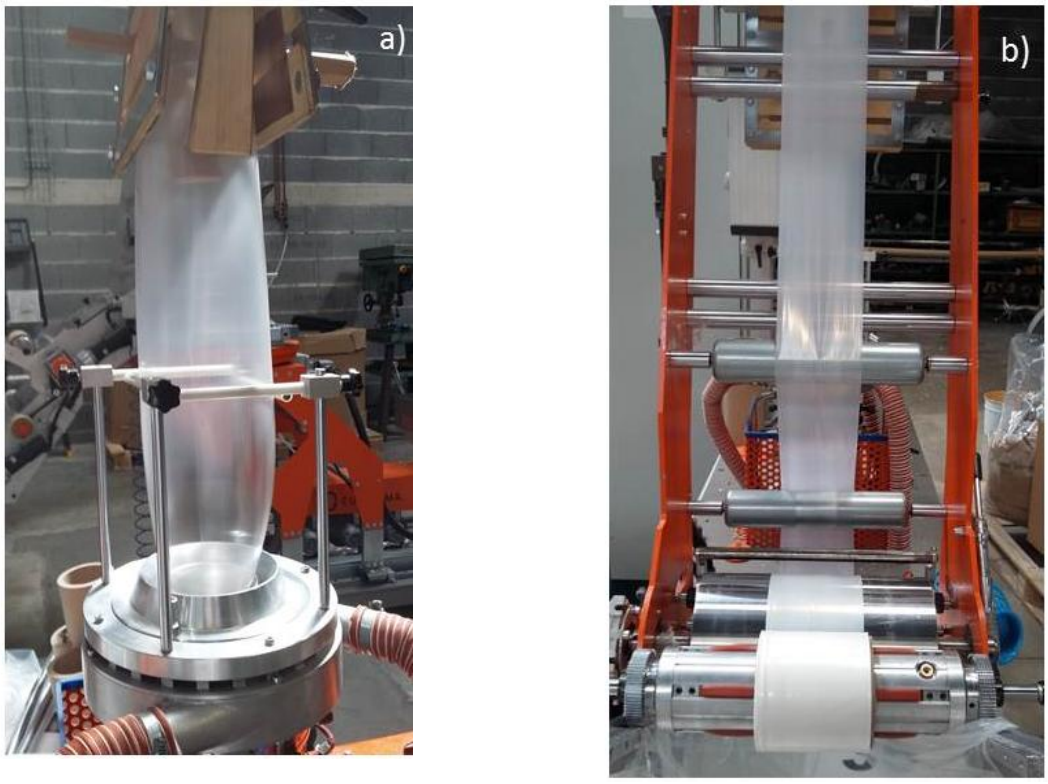

538 **Fig. 11.** Photographies of the PBS-Mg_2Al/HPP composite at a) the output of the fan extruder,
539 and b) the exit of roll.

540

541 **CONCLUSION**

542 As usual LDH appears in this study as an adaptive toolbox in combination with interleaved
543 organic molecules of interest for desired application. The combination of two LDH filler
544 associating anions HPP and ASA appears as an efficient compromise to perform against photo-

aging and hydrolysis of PBS, as well as cancelling the bacteria activity, this by keeping an improved chain extension effect, superior to LDH-HPP itself. It is worth to mention that ASA molecules is known to suffer from temperature and light, it appears to be less sensitive and protected when ensconced into LDH gap.

A technological scale-up to produce larger amount of PBS composite than in the laboratory frame is possible. The obtained thin film is found to be more resistant to extension and tearing, that is highly suitable for flexible packaging, and keeping most of the properties of the PBS intact. Evidently, one of the drawbacks is the high WVTR that needs to be strongly diminished compared to PBS free of filler, thus weakening for now a possible direct applicability, but keeping open the cases where the barrier to water is not the main requirement.

ASSOCIATED CONTENT

Supporting Information

The Supporting Information includes: TGA and DTGA traces of obtained PBS nanocomposites, XRD patterns of PBS nanocomposites with 10 wt. % of Mg-Al organo-modified LDHs, UV-vis transmittance and fluorescence spectra of PBS and PBS composites with 5 wt. % of Mg-Al organo-modified LDHs during photo-degradation at 60 °C, evolution of Newtonian zero-shear viscosity η'_0 and succinic acid concentration during hydrolysis of PBS and PBS-Mg-Al LDH composites at 50 °C.

Author Contributions

F.L. and V.V. conceived the project. A.A.M. prepared the samples and performed UV-ageing and hydrolysis experiments. G.T., L.S. and A.C. were responsible for DSC and TGA analysis, while A.A.M. carried out the rheology, UV-vis, SEM, XRD and fluorescence measurements. N.B.C. and D.G determined antibacterial properties. A.A.M and F.L. analyzed the data and prepared the manuscript. All authors contributed to the discussion of the results. All authors have given approval to the final version of the manuscript.

ACKNOWLEDGMENT

The authors thank CNRS / DIRE for the financial support for research and founding a postdoc position for Adam Marek (2016–2017) through the project PREMAT n°116. The authors would like to thank P. Breuilles, S. Essabaa and S. Guerreiro, all from CNRS, for their fruitful discussions, as well as L. Saint Macary (SATT GC) and SATT GC for the scale-up funding.

The authors thank also G. Voyard, R. Thirouard, R. Turczyn and N. Caperaa for their help in using the apparatus for XRD, ionic chromatography, SEM analysis and LDH scale-up synthesis, respectively.

REFERENCES

Aisawa, S., Higashiyama, N., Takahashi, S., Hirahara, H., Ikematsu, D., Kondo, H., Nakayama, H., Narita, E., (2007). Intercalation behavior of L-ascorbic acid into layered double hydroxides. Appl. Clay Sci. 35, 146–154.

Al-Salem, S. M., Lettieri, P., Baeyens, J., (2010). The valorization of plastic solid waste (PSW) by primary to quaternary routes: From re-use to energy and chemicals. Prog. Energ. Combust. Sci. 36, 103–129.

Bimestre, B. H., Saron, C., (2012). Chain extension of poly (ethylene terephthalate) by reactive extrusion with secondary stabilizer. Mater. Res. 15, 467–472.

Bittner, S., (2006). When quinones meet amino acids: chemical, physical and biological consequences. Amino Acids. 30, 205-224.

Cavani, F., Trifiró, F., Vaccari, A., (1991). Hydrotalcite-type anionic clays: Preparation, properties and applications. Catal. Today 11, 173–301.

Chan, D. I., Prenner, E. J., Vogel, H. J., (2006). Tryptophan- and arginine-rich antimicrobial peptides: Structures and mechanisms of action. Biochim. Biophys. Acta. 1758, 1184–1202.

Coelho, C., Stimpfling, T., Leroux, F., Verney, V., (2012). Inorganic–Organic Hybrid Materials Based on Amino Acid Modified Hydrotalcites Used as UV Absorber Fillers for Polybutylene Succinate. Eur. J. Inorg. Chem. 5252–5258.

Costantino, U., Bugatti, V., Gorrasi, G., Montanari, F., Nocchetti, M., Tammaro, L., Vittoria, V., 2009. New Polymeric Composites Based on Poly(epsilon-caprolactone) and Layered Double Hydroxides Containing Antimicrobial Species. ACS Applied Mater. Inter. 1, 668-677.

Demirkaya, Z. D., Sengul, B., Eroglu, M. S., Dilsiz N., (2015). Comprehensive characterization of polylactide-layered double hydroxides nanocomposites as packaging materials. J. Polym. Res. 22, 124.

Friedrich, C., Braun, H. (1992). Generalized Cole-Cole behavior and its rheological relevance. Rheol. Acta 31, 309–22.

Gao, X., Lei, L., O'Hare, D., Xie, J., Gao, P., Chang, T., (2013). Intercalation and controlled release properties of vitamin C intercalated layered double hydroxide. J. Solid State Chem. 203, 174–180.

Gigli, M., Fabbri, M., Lotti, N., Gamberini, R., Rimini, B., Munari, A., (2016). Poly(butylene succinate)-based polyesters for biomedical applications: A review. Eur. Polym. J. 75, 431–460.

Kim, H.-S., Yang, H.-S.-, Kim, H.-J., (2005). Biodegradability and mechanical properties of agro-flour-filled polybutylene succinate biocomposites. J. Appl. Polym. Sci. 97, 1513-1521.

Lala, N. L., Ramaseshan, R., Bojun, L., Sundarrajan, S., Barhate, R. S., Ying-jun, L., Ramakrishna, S., (2007). Fabrication of nanofibers with antimicrobial functionality used as filters: protection against bacterial contaminants. Biotechnol. Bioeng. 97, 1357–1365.

Leroux, F., Verney, V., Sisti, L., Celli, A., Totaro, G. (2017). Organo-modified LDH and composite polymer materials comprising same. PCT patent 15/576,459.

Mark-Houwink Equation. (2007). In Polymer Chemistry, 2nd ed.; Hiemenz, P.C.; Lodge, T. P., Ed.; CRC Press: Boca Raton. 336–341.

Park, E. S., (2015). Antimicrobial polymeric materials for packaging applications: A review. In The Battle Against Microbial Pathogens: Basic Science, Technological Advances and Educational Programs; Méndez-Vilas, A., Ed.; Formatex Research Center: Badajoz, 1, 500–511.

Rhim, J–W., Park, H-M., Ha, C–S., (2013). Bio-nanocomposites for food packaging applications. Prog. Polym. Sci. 38, 1629–1652.

Rives, V., Ulibarri, M. A., (1999). Layered double hydroxides (LDH) intercalated with metal coordination compounds and oxometalates. Coord. Chem. Rev. 181, 61–120.

Salo, R. J., Cliver, D. O., (1978). Inactivation of enteroviruses by ascorbic acid and sodium Bisulfite. Appl. Environ. Microbiol. 36, 68–75.

Sun, J., Lin, Y., Shen, X., Jain, R., Sun, X., Yuan, Q., Yan, Y., (2016). Aerobic biosynthesis of hydrocinnamic acids in Escherichia coli with a strictly oxygen-sensitive enoate reductase. Metab. Eng. 35, 75–82.

The New Plastics Economy: Rethinking the future of plastics, World Economic Forum, January 2016.

Totaro, G., Sisti, L., Celli, A., Askanian, H., Hennous, M., Verney, V., Leroux, F., (2017). Chain extender effect of 3-(4-hydroxyphenyl)propionic acid/layered double hydroxide in PBS bionanocomposites. Eur. Polym. J. 94, 20–32.

Totaro, G., Sisti, L., Celli, A., Aloisio, I., Di Gioia, D., Marek, A. A., Verney, V., Leroux, F., (2018). Dual chain extension effect and antibacterial properties of biomolecules interleaved within LDH dispersed into PBS by in situ polymerization. Dalton Trans. 47, 3155–3165.

Wei, M., Yuan, Q., Evans, D. G., Wang, Z., Duan, X., (2005). Layered solids as a “molecular container” for pharmaceutical agents: L-tyrosine-intercalated layered double hydroxides. J. Mater. Chem. 15, 1197–1203.

Wei, Z., Chen, G., Shi, Y., Song, P., Zhan, M., Zhang, W., (2012). Isothermal crystallization and mechanical properties of poly(butylene succinate)/layered double hydroxide nanocomposites. J. Polym. Res. 19, 9930.

Xie, J., Zhang, K. Wu, J., Ren, G., Chen, H., Xu, J., (2016). Bio-nanocomposite films reinforced with organo-modified layered double hydroxides: Preparation, morphology and properties. Appl. Clay Sci. 126, 72–80.

E.S. Yoo and S.S. Im, (1999). Melting behavior of poly(butylene succinate) during heating scan by DSC. J. Polym. Sci., Part B: Polym. Phys. 37, 1357–1366.